Available online at www.sciencedirect.com
SCIENCE DIRECT®
Journal of Nuclear Materials 335 (2004) 302–310
journal of nuclear materials
www.elsevier.com/locate/jnucmat

Solid state synthesis of Mg–Ni ferrite and characterization by XRD and XPS

V.K. Mittal [a], Santanu Bera [a], R. Nithya [b], M.P. Srinivasan [a], S. Velmurugan [a], S.V. Narasimhan [a,*]

[a] *Water and Steam Chemistry Laboratory, BARC Facilities, IGCAR Campus, Bhabha Atomic Research Centre, Kalpakkam 603 102, Tamil Nadu, India*

[b] *Materials Science Laboratory, IGCAR, Kalpakkam 603 102, Tamil Nadu, India*

Received 14 October 2003; accepted 2 May 2004

Abstract

Single-phase magnesium–nickel ferrites with varying amounts of nickel and magnesium were characterized by X-ray diffraction (XRD) and X-ray photoelectron spectroscopy (XPS) techniques. A plot of lattice parameter versus composition of the ferrites ($Mg_xNi_{(1-x)}Fe_2O_4$, $x \leqslant 1$) showed an abrupt deviation of lattice parameter linearity near $MgFeO_4$. The deviation was explained in terms of the distribution of Mg^{2+} in the octahedral and tetrahedral sites of the oxygen lattice. In XPS spectra, a broadening of the Mg 1s peak in Ni rich Mg–Ni ferrites from that observed in pure $MgFe_2O_4$, was explained by changes in the distribution of Mg^{2+} ion in tetrahedral and octahedral sites. A depth distribution of Mg in $Ni_{0.5}Mg_{0.5}Fe_2O_4$ showed an enrichment of Mg on surface.

1. Introduction

In pressurized heavy water reactors (PHWRs), the radioactive isotopes of cobalt, viz. Co^{58} and Co^{60}, are primarily responsible for the radiation field build-up in the primary heat transport (PHT) system. Controlling the exposure of power plant personnel to this radiation is a task for the power plant operators. These isotopes are formed by the neutron activation of the nickel and cobalt containing corrosion products that are transported to the core during the operation of the reactor. The formation of corrosion product on the out-of-core surfaces, transportation to the core by the coolant and deposition on the out-of-core surfaces are controlled by several factors. Ferrites having spinel structure such as magnetite and nickel ferrite etc., dominate the corrosion product oxide inventory in PHWRs and hence they play a major role in the activity transport process. Thus, attempts are being made to study the various ferrites of relevance to nuclear reactor water coolant systems and to evaluate the impact of substitution of the divalent metal ions normally present in the coolant system structural materials with extraneous divalent metal ions to modify the properties of these oxides. It was observed [1] that the presence of Zn^{2+} ion at ppb (5–15 ppb) level in boiling water reactor (BWR), remarkably reduced the radiation build-up in the coolant circuits. The mechanism proposed for reduction in radiation build-up in the presence of Zn^{2+} ion includes the formation of a modified layer of ferrite containing zinc ions which offers additional apparent passivity [2]. This reduces the release of corrosion products to the coolant thereby reducing the extent of contamination. Since Zn^{64} has a high cross section for neutron absorption to produce γ-emitting Zn^{65} ($t_{1/2} = 244$ d), it partially offsets the

* Corresponding author. Tel.: +91-4114 280097; fax: +91-4114 280097/280203.
E-mail address: svn@igcar.ernet.in (S.V. Narasimhan).

0022-3115/$ - see front matter © 2004 Elsevier B.V. All rights reserved.
doi:10.1016/j.jnucmat.2004.05.010

reduction in radiation level achieved by the addition of zinc. Also, it aggravates the problem of radioactive waste management. Hence, the power plants have to switch over to very expensive ^{64}Zn depleted zinc treatment. In addition, when studies were conducted under the chemistry conditions of the PHWR coolant system, zinc did not show any observable passivation effect. Thus there is a need for an alternative to Zn, which should have properties similar to zinc but more effective in reducing the radiation field in PHWRs. As zinc and magnesium have similar properties by virtue of their position in the periodic table, it was felt that magnesium can be used as a substitute [3] for zinc ion in reducing the radioactivity build-up. Experiments carried out under simulated PHWR PHT system conditions indicated that the thickness of the oxide formed over carbon steel and Incoloy-800 were low when magnesium was present in the water [3]. Also, in both alloys significant concentration of magnesium could be detected using X-ray photoelectron spectroscopic technique.

In the temperature conditions (~300 °C) prevailing in the coolant systems of power reactors, normally mixed ferrites of composition $M_xFe_{(3-x)}O_4$ (where M is a divalent metal ion viz. Ni^{2+}, Co^{2+} etc.) is formed. The value of 'x' range from 0–1 and it varies from material to material. In systems containing chromium, the oxide film would also contain chromites. These ferrites have spinel ($MgAl_2O_4$) like structure. The divalent and trivalent metal ions each occupy either the octahedral or tetrahedral or both sites present in the oxide lattice. In a ferrite having the normal spinel structure, the divalent metal ion occupies the tetrahedral site where as the trivalent Fe^{3+} ion occupies the octahedral site. In ferrites having inverse spinel structure, the divalent metal ion goes to the octahedral site.

Cation distribution in tetrahedral and octahedral sites of ferrites can affect the pick up of active metals ions from the solution into these spinels [4]. The dependence of cation distribution in ferrites on temperature has been reported by several groups [4,5]. It was observed that the cation distribution in spinel is influenced by the bimetallic composition of the ferrite spinel even at room temperature and hence likely to influence the pick up of active materials. In the process of Mg ion passivation, Mg ferrite crystallites are expected to form as the passive layer in a randomly distributed manner. On the other hand, monel (70Ni–30Cu) or Incoloy-800 steam generator tubes of PHWR reactors release Ni (ppb level) into the circuit water at high temperature. Hence, during passivation of the coolant system by magnesium ion, mixed ferrites containing both Mg^{2+} and Ni^{2+} are likely to form in the passive layer. Thus, it is important to know the cation distribution in Mg–Ni ferrites prior to the investigation on mechanism involved in passivation or radioactive ions pick up in PHT system of PHWR type reactor.

The ferrite deposited in the coolant circuits of the power plants is formed by the reaction of high temperature water with the metal surfaces. In order to understand the behavior of these ferrites, studies have been carried out by synthetically preparing these ferrites using either hydrothermal synthesis methods or by high temperature solid state synthesis methods. Model corrosion products such as $NiFe_2O_4$ and Fe_3O_4 were prepared by solid state method and studied by XRD technique to identify the nature and origin of corrosion products in the coolant circuits [6]. Dissolution mechanisms of the ferrites were studied [7] to find a suitable organic solution to dissolve radioactive nuclides of the coolant circuit of the power plant using ferrites prepared by the high temperature solid state method. This study also indicated the magnetite prepared by the hydrothermal route behaves similar to the one prepared by solid state method. Thus, the high temperature solid state method of preparation of ferrites has been found to give ferrites of required purity, stoichiometry and with solid state characteristics similar to the ferrites formed as corrosion products on the reactor coolant system surfaces. Hence, the ferrites prepared by this method can be used as a model corrosion product to study their behavior.

In the present report, $Mg_xNi_{(1-x)}Fe_2O_4$ powder was prepared by solid state reaction method. Pure stoichiometric ferrite required for investigating the cation distribution could be prepared through solid state synthesis technique. The observations of cation distribution in the powder $Mg_xNi_{(1-x)}Fe_2O_4$ can be utilized for real system ferrites of the coolant circuits. XPS and XRD techniques are widely used as characterization tools for identifying the phase and chemical state of ferrites [3,6,8,9]. In this study, Mg–Ni ferrite powder with different composition was prepared by high temperature solid state method to get very pure ferrites. The samples were analyzed by XRD to confirm the formation of Mg–Ni ferrites. The distribution of Mg ions in octahedral and tetrahedral sites was observed by XPS.

2. Experiment

2.1. Sample preparation

The $Mg_xNi_{1(-x)}Fe_2O_4$ ($x = 0$, 0.2, 0.3, 0.5, 0.7, 0.9, 1) ferrite samples were prepared by solid state route at high temperature. An appropriate amount (Table 1) of $MgCO_3$, $NiCO_3$. $2Ni(OH)_2 \cdot 4H_2O$ and α-Fe_2O_3 were thoroughly mixed with acetone to homogenize the mixture prior to the solid state formation of Mg ferrite and Mg–Ni ferrite. The pellets (diameter 10 mm) formed at 65 kN/cm^2 pressure were put in a silica boat and annealed in a re-crystallized alumina tubular furnace at 1200 °C for 12 h in air. Air purging was continuous through out the heating process. Subsequent to the first

Table 1
Preparation of $MgFe_2O_4$, $Mg_xNi_{(1-x)}Fe_2O_4$ and $NiFe_2O_4$

Ferrite	α-Fe_2O_3 (in wt%)	$MgCO_3$ (in wt%)	$NiCO_3 \cdot 2Ni(OH)_2 \cdot 4H_2O$ (in wt%)
$NiFe_2O_4$	56.02	–	43.98
$Ni_{0.8}Mg_{0.2}Fe_2O_4$	57.68	6.10	36.22
$Ni_{0.7}Mg_{0.3}Fe_2O_4$	58.55	9.27	32.18
$Ni_{0.5}Mg_{0.5}Fe_2O_4$	60.37	15.93	23.70
$Ni_{0.3}Mg_{0.7}Fe_2O_4$	62.30	23.02	14.68
$Ni_{0.2}Mg_{0.8}Fe_2O_4$	63.31	26.75	9.94
$Ni_{0.1}Mg_{0.9}Fe_2O_4$	64.36	30.58	5.06
$MgFe_2O_4$	65.45	34.55	–

heating, the pellets were ground and homogenized with acetone. Again pellets were formed at 85 kN/cm^2 pressure for sintering at 1200 °C for 18 h. $NiFe_2O_4$ was prepared by heating reactants at 950 °C for 12 h and subsequently sintering at 1000 °C for 18 h. For preparation of nickel ferrite, magnesium ferrite and magnesium–nickel ferrite the heating rate of the furnace was 3 °C/min and the cooling rate was 3.3 °C/min to cool up to 500 °C and then it was furnace cooled.

2.2. Characterization

The XPS system used for this study was a VG ESCALAB MK200X system, with 150 mm hemispherical analyzer. The spectra were collected using Al K_α X-ray source and with 20 eV pass energy of the analyzer. The data acquisition and processing were carried out using Eclipse software. The instrument was calibrated with Au $4f_{7/2}$ line at 84.0 eV with 1.6 eV FWHM [10]. The ferrite pellets were mechanically etched to avoid any surface contamination that might have occurred due to pelletization before loading for the XPS analysis. The C 1s peak of the contaminants was taken as 285.0 eV for charging correction.

X-ray diffraction patterns of the powder samples were recorded by STOE (Germany) X-ray diffractometer using Cu K_α as incident radiation at a 2θ scan rate of 0.1°/5 s in 10–100° span.

3. Results and discussion

Magnesium ferrite powder is brown in color and gradually becomes black as its composition changes from Mg rich Mg–Ni ferrite to Ni rich ferrite. $MgFe_2O_4$ is an inverse spinel but at room temperature itself about 10% of it exists in normal spinel form. The structural formula of $MgFe_2O_4$ is written as $[Mg_{(1-y)}Fe_y]_A[Mg_yFe_{(2-y)}]_BO_4$ (A = tetrahedral, B = Octahedral) depending on the degree of inversion. Studies carried out on $MgFe_2O_4$ with Mössbauer indicated the distribution of Mg ions in octahedral and tetrahedral sites and the distribution was found to vary with duration of milling [11] and with quenching temperature in the range 100–1400 °C [12]. Nickel ferrite is an inverse spinel and hence the Ni^{2+} occupies only octahedral site of the cubic lattice.

3.1. X-ray diffraction

The XRD pattern for stoichiometric mixture of α-Fe_2O_3 and $MgCO_3$ is shown in Fig 1(a). The main diffraction peaks for $MgCO_3$ occurs at 2θ values 33.6 and 53.89 but were seen coinciding with the main peaks of α-Fe_2O_3. Fig 1(b) shows the formation of spinel structure after heating the stoichiometric mixture at 1200 °C. The lattice parameter was measured and was found to be 0.8393 nm, which is in agreement with the reported value of 0.8387 nm for the $MgFe_2O_4$ [13]. The lattice parameter of Fe_3O_4 is 0.8397 nm [6]. According to the report by O'Neill et al. [6], the lattice parameter of $MgFe_2O_4$ varies between the values 0.838–0.840 nm; hence it is not possible to distinguish Fe_3O_4 and $MgFe_2O_4$ by XRD. However, no Fe_3O_4 was detected by XPS technique (discussed later). The possibility of formation of γ-Fe_2O_3 was ruled out, as the lattice parameter of γ-Fe_2O_3 is 0.8339 nm, which is very much less

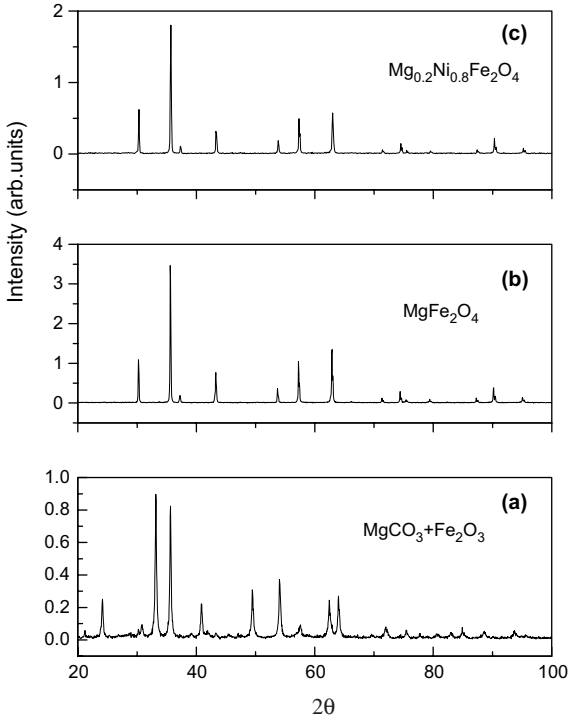

Fig. 1. X-ray diffraction patterns for (a) mixture of $MgCO_3$ and Fe_2O_3, (b) $MgFe_2O_4$ spinel after heating the mixture to 1200 °C for 30 h and (c) $Mg_{0.2}Ni_{0.8}Fe_2O_4$.

than the $MgFe_2O_4$ and any solution of γ-Fe_2O_3 and $MgFe_2O_4$ would have resulted in lowering the lattice parameter.

In ferrites, Ni^{2+} and Mg^{2+} are preferred in the octahedral sites of oxygen lattice. The ionic radii of Ni^{2+} and Mg^{2+} in octahedral site are 0.069 and 0.072 nm respectively [14]. Hence it is expected that the lattice parameter of the Mg–Ni ferrite would increase with the increase in Mg content in the spinel. In Fig. 2, the plot of the lattice parameter obtained from different composition of Mg and Ni is shown. Although the lattice parameter was seen increasing linearly with the Mg content in the ferrite, the lattice parameter of $MgFe_2O_4$ deviated from the expected line (dotted) as shown in Fig. 2. In case of Fe–Mo–Ti–O spinel, the lattice parameter was reported to follow the Vegard's rule of linearity with different composition of Mo and Ti [15]. In case of Ni–Zn ferrites [16] the linearity of the lattice parameter was shown with different composition of Ni and Zn. But in this case, the lattice parameter showed an abrupt deviation from the linearity near $MgFe_2O_4$ (Fig. 2). In general, a cation disorder develops in $MgFe_2O_4$ when it is prepared by solid state method [6]. It was reported [11] that around 10% of Mg^{2+} were distributed in tetrahedral sites of the spinel during synthesis. Such disorder of Mg^{2+} might be the reason for the enhanced lattice parameter [6].

3.2. X-ray photoelectron spectroscopy

The surface of the sample was characterized by XPS after calibrating the spectrometer. The binding energy of Mg 1s peak from standard MgO was found to be 1303.6 eV, which matches well with the literature value [17] and the atomic concentration ratio of Mg and O was 47:53. The concentration of oxygen in the sample was slightly more than the expected value due to physisorbed O on the sample surface.

The atomic concentration ratio of the total (Mg + Ni) to Fe in $Mg_xNi_{(1-x)}Fe_2O_4$ was seen matching well with the stoichiometry of the compound. But, the Mg:Ni ratio was seen to be varying with the amount of Mg content in the sample.

In Fig. 3, Mg/Ni atomic concentration ratio of $Mg_xNi_{(1-x)}Fe_2O_4$ obtained from XPS is shown as a function of composition (x). It appears from the graph that the surface is enriched with Mg and the enrichment increases with Mg content in the material. For $Mg_{0.5}Ni_{0.5}Fe_2O_4$, the surface composition was observed to be $Mg_{0.65}Ni_{0.35}$, where Mg was more than the

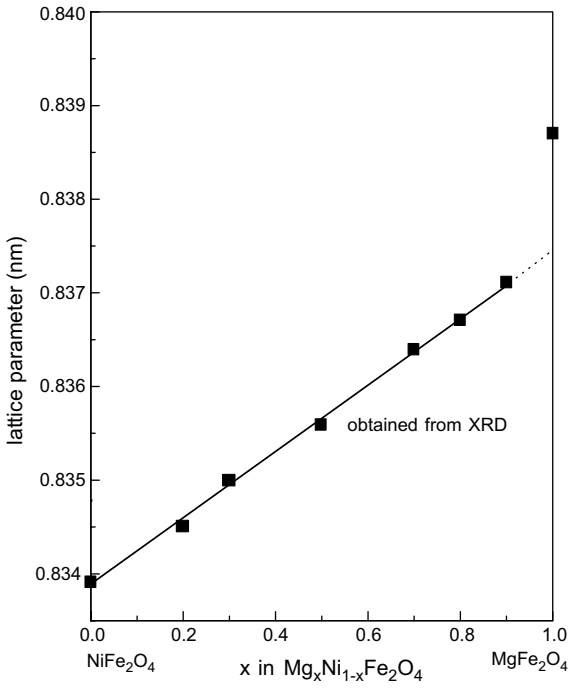

Fig. 2. Lattice parameters calculated from X-ray diffraction patterns plotted as a function of Mg content in the spinel series $Mg_xNi_{(1-x)}Fe_2O_4$. The lattice parameter of $MgFe_2O_4$ is seen deviated from the line due to cation disorder of Mg^{2+} in the ferrite.

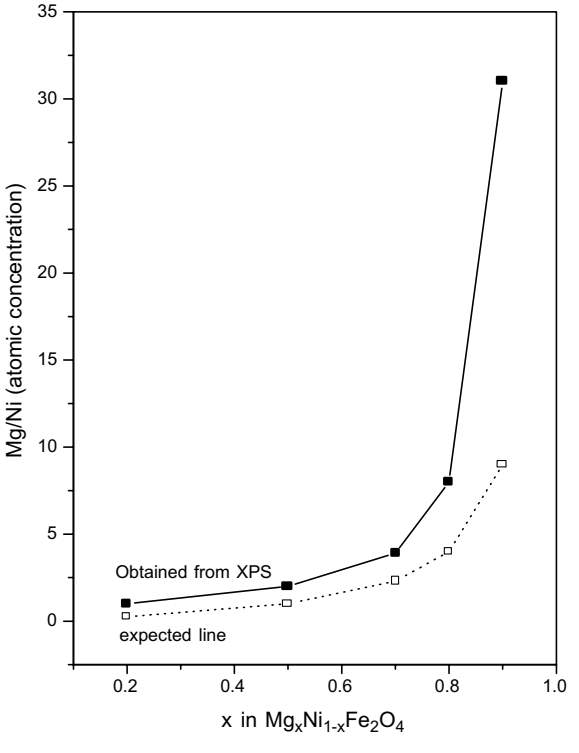

Fig. 3. (Mg/Ni) atomic concentration ratio of surface of $Mg_xNi_{(1-x)}Fe_2O_4$ ferrites as a function of Mg content. It showed that Mg is highly enriched on the surface in case of Mg rich ferrites.

expected amount. Such variation of the Mg content along the depth of the grains was further confirmed by performing XPS depth profiling of the $Mg_{0.5}Ni_{0.5}Fe_2O_4$ grains. It is shown in Fig. 5(d) that the surface of the ferrite grains is enriched with Mg and it decreased on sputtering and finally attained a saturation value. The average sputtering rate was 0.2 nm per minute and the sputtering current was maintained at 2.0 μA with 2.0 keV beam energy.

3.2.1. Mg 1s peak analysis

The binding energy of photoelectron peak is not only dependent on the chemical state of the atoms, but also on its molecular environment. In case of Ni^{2+} in NiO, the binding energy of Ni $2p_{3/2}$ was seen at 854.0 eV where as in $NiFe_2O_4$ it was 855.4 eV [18]. Similarly, the binding energy of $2p_{3/2}$ of Zn^{2+} in the tetrahedral site of $ZnFe_2O_4$ was seen at 1021.4 eV and that in octahedral site it was around 1023.2 eV [8]. Thus, in ferrites, when cations are distributed in two different sites, two XPS peaks or a peak broadening of the photoelectron peak is expected. The difference in binding energy is attributed to the difference in the stabilization between two sites due to difference in co-ordination and lattice effects. In case of $MgFe_2O_4$, the peak position of Mg 1s has not been studied so far. In $MgFe_2O_4$, Mg is incorporated in octahedral site of the spinel. The binding energy of MgO is observed to be 1303.6 eV and was seen reduced to 1303.1 eV in $MgFe_2O_4$. The atomic concentration of Mg and Fe was calculated to be 32:68, which is in good agreement with the atomic ratio of the cation in $MgFe_2O_4$. The small shift in binding energy of Mg^{2+} 1s peak in ferrite in comparison to that in MgO is due to the different surrounding in which the Mg ion is placed in the two compounds that contribute to the difference in relaxation effect.

Mg 1s in $Mg_xNi_{(1-x)}Fe_2O_4$ was studied extensively to find the Mg^{2+} distribution in tetrahedral and octahedral sites. In Table 2, the binding energy and other peak parameters are shown. The peak width of the Mg 1s in $MgFe_2O_4$ was 2.1 eV and almost symmetric. When $MgFe_2O_4$ was annealed for one hour at 1000 °C to establish equilibrium of cation disorder, and quenched to ice temperature, Mg 1s peak width increased to 3.4 eV. The cation distribution of Mg^{2+} in octahedral and tetrahedral sites on heat treatment was shown by O'Neill et al. [6] by using XRD and Mössbauer spectroscopy. So the increase in the peak width of XPS peak was attributed to the distribution of the Mg ions in octahedral and the tetrahedral sites of the spinel.

In Fig. 4 the deconvoluted spectrum of the Mg 1s for the quenched sample is shown. A peak at 1302.2 eV (FWHM 2.1 eV) was obtained along with the peak at 1303.3 eV (FWHM 2.2 eV) after deconvolution. The higher energy peak corresponds to pure Mg ferrite and is associated with the octahedral Mg ions, and the lower energy peak is due to the Mg ions in the tetrahedral site. The reduction in the binding energy in case of tetrahedral Mg^{2+} was due to lower number of O^{2-} ions surrounding the tetrahedral site. Similar distribution of Zn ions was seen by XPS in $ZnFe_2O_4$ [8].

In $Mg_xNi_{(1-x)}Fe_2O_4$ ferrite the peak width of Mg 1s was increased (shown in Table 2) due to the incorporation of Ni in the spinel. Such increase in peak width is also interpreted as due to cation distribution of Mg^{2+} in two different sites, which is influenced by the presence of Ni^{2+} in the ferrite. Cation distribution in $Mg_xNi_{(1-x)}Fe_2O_4$ was also observed during measurement of the magnetic property of these ferrites [19]. In Fig. 5(c) and (d), Mg 1s peaks are deconvoluted into two peaks to show its distribution in octahedral and tetrahedral sites of the spinel. It was seen that the Mg distribution in tetrahedral site is around 35% of the total Mg^{2+} content in $Ni_{0.5}Mg_{0.5}Fe_2O_4$. Nickel is always preferred in octahedral sites and it occupies the octahedral site during the ferrite growth. As Fe^{3+} and Mg^{2+} can enter into both sites, these two cations have distributed themselves in those two sites. When Ni amount was small (as in case of

Table 2
Binding energy (BE) of Mg 1s photoelectron peak in different samples

Sample	BE Mg 1s (FWHM), in eV	BE O 1s, in eV	BE Fe $2p_{3/2}$ in eV	BE Ni $2p_{3/2}$ (FWHM) in eV
MgO	1303.6 (2.5)	530.5		
$MgFe_2O_4$	1303.1 (2.1)	529.9	711.2	
Quenched $MgFe_2O_4$	1302.5 (3.4)	529.8	710.6 satellite (8.0-9.0)	
$MgFe_2O_4$ sputtering	1303.2 (2.1)		710.5 satellite vanished	
$NiFe_2O_4$		530.2	711.2 satellite (8.0–9.0)	855.1 (2.0) satellite 6.5
$Mg_{0.9}Ni_{0.1}Fe_2O_4$	1303.1 (2.4)	529.7	711.0 satellite (8.0–9.0)	854.7 (1.9) satellite 6.5
$Mg_{0.8}Ni_{0.2}Fe_2O_4$	1303.3 (2.2)	530.2	711.2 satellite (8.0–9.0)	855.2 (1.8) satellite 6.5
$Mg_{0.7}Ni_{0.3}Fe_2O_4$	1303.3 (2.4)	529.7	710.8 satellite (8.0–9.0)	854.7 (2.0) satellite 6.5
$Mg_{0.5}Ni_{0.5}Fe_2O_4$	1302.6 (2.7)	529.8	710.5 satellite (8.0–9.0)	854.7 (2.2) satellite 6.5
$Mg_{0.3}Ni_{0.7}Fe_2O_4$	1303.1 (3.1)	529.5	710.5 satellite reduced	854.3 (2.0) satellite 6.5
$Mg_{0.2}Ni_{0.8}Fe_2O_4$	1303.1 (3.4)	529.4	710.5 satellite reduced	854.1 (2.0) satellite 6.5

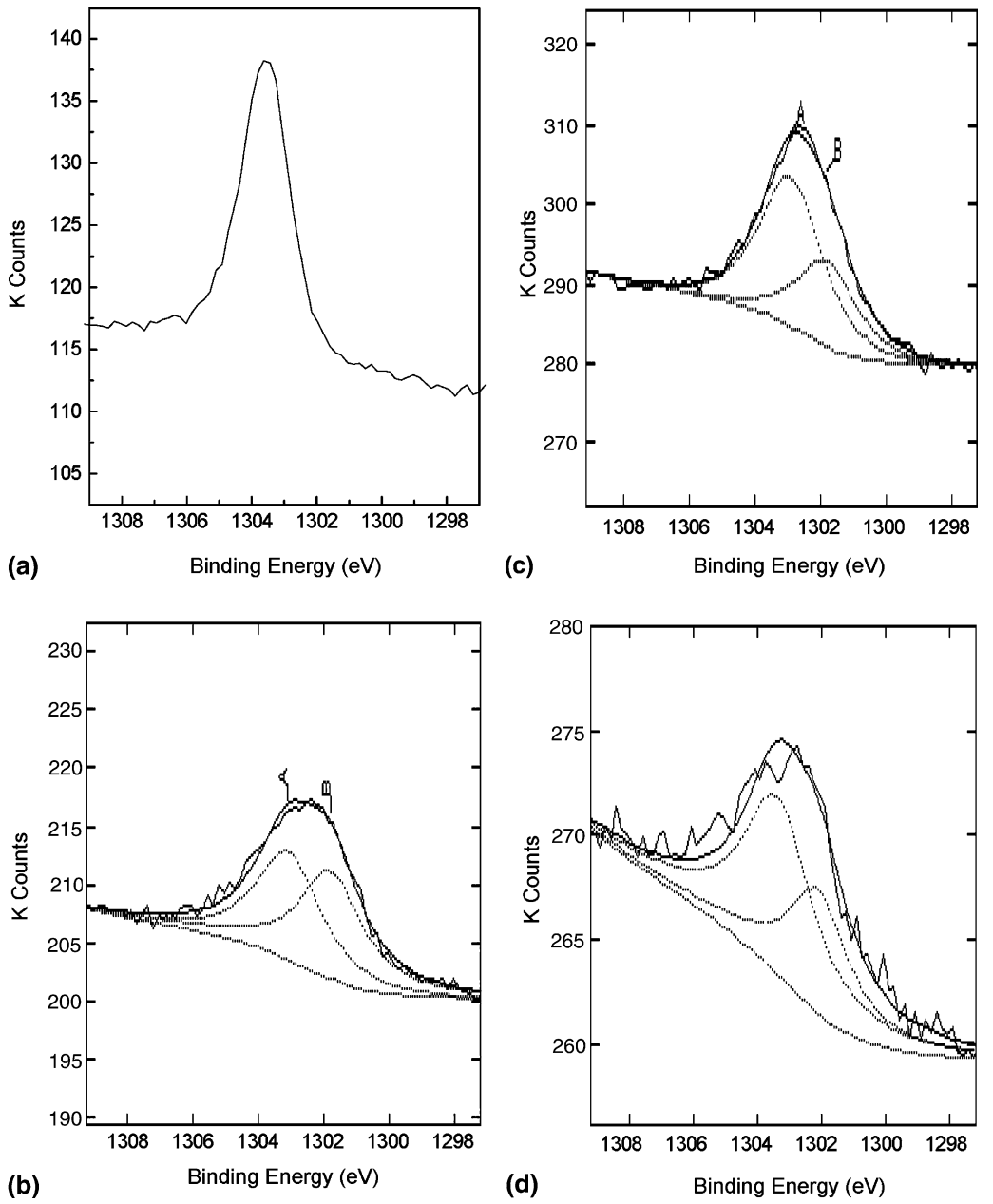

Fig. 4. Mg 1s photoelectron peak from (a) $MgFe_2O_4$, (b) deconvoluted Mg 1s peak after quenching the sample at 1000 °C, (c) deconvoluted Mg 1s peak from $Mg_{0.5}Ni_{0.5}Fe_2O_4$ and (d) deconvoluted Mg 1s peak from $Mg_{0.3}Ni_{0.7}Fe_2O_4$.

$Mg_xNi_{(1-x)}Fe_2O_4$, $x = 0.9$, 0.8, 0.7) the Mg 1s peak width did not change much, as the majority of Mg ions are placed in the octahedral site. However, a thorough analysis is required to find the distribution of Mg^{2+} as a function of Ni content in the ferrite.

3.2.2. Fe 2p photoelectron peak analysis

In Table 2, the binding energy values of Fe $2p_{3/2}$ in the ferrites are shown. The binding energy of Fe $2p_{3/2}$ was 711.2 eV for pure magnesium ferrite. However in Mg–Ni ferrites the binding energy values were found in a range from 711.2 to 710.5 eV. In all those ferrites, the presence of Fe^{3+} was detected and was confirmed by its distinct characteristic satellite peak at around 8.0 eV above the principal peak. Magnetite (Fe_3O_4) does not show any satellite [8] due to overlapping of the satellite peaks for Fe^{3+} (at 8.0 eV) and Fe^{2+} (at 6.0 eV) resulting in the formation of a broad background. Thus, the

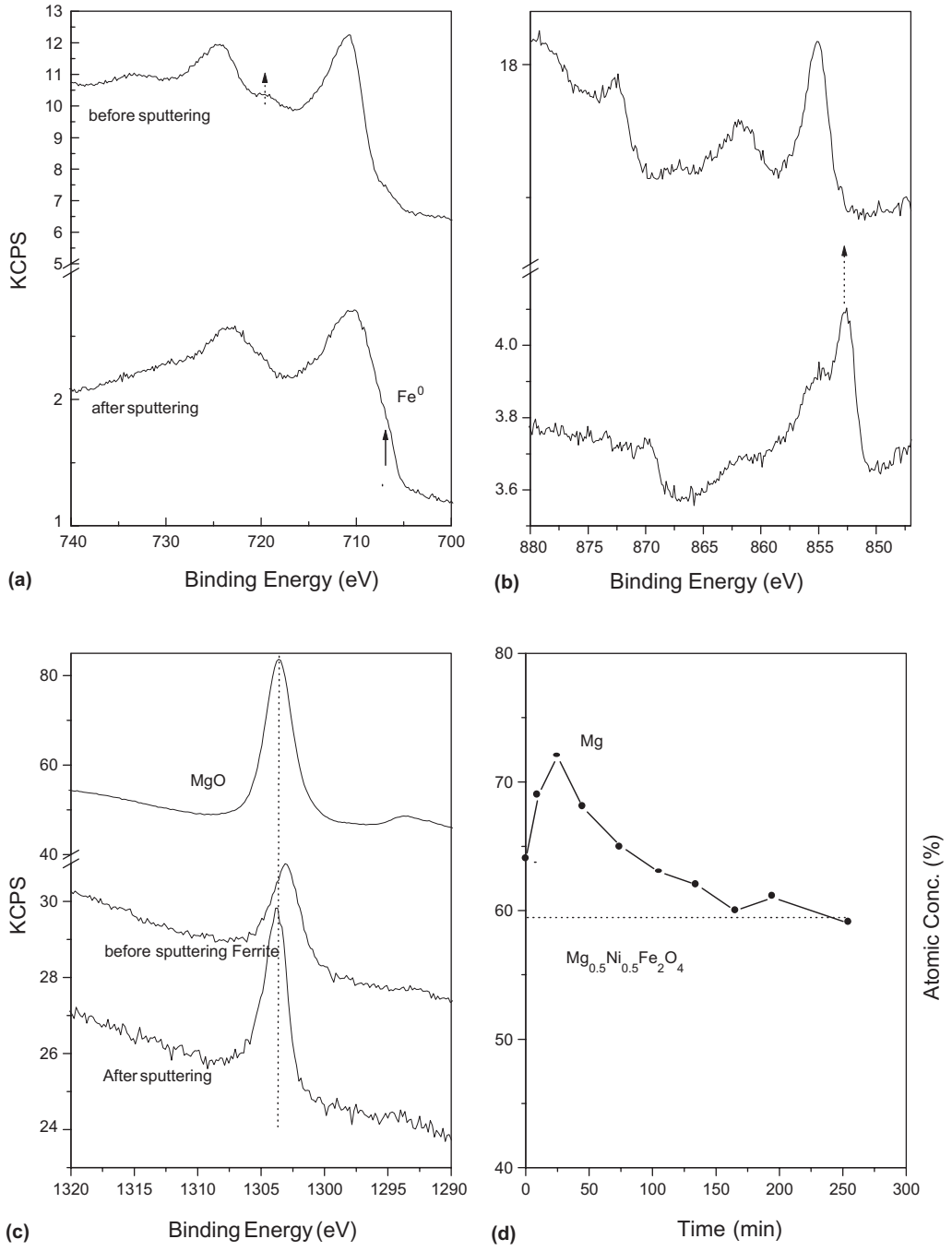

Fig. 5. Sputtering effects on $Mg_{0.5}Ni_{0.5}Fe_2O_4$: (a) Fe 2p photoelectron peak, the satellite was vanished (arrow) after sputtering, (b) Ni 2p photoelectron peak, Ni^0 appeared after sputtering (arrow), (c) Mg 1s photoelectron peak from the samples MgO, $Mg_{0.5}Ni_{0.5}Fe_2O_4$ and (d) depth distribution of Mg in $Mg_{0.5}Ni_{0.5}Fe_2O_4$.

observation of a distinct satellite at 8.0 eV above the main peak indicated the absence of Fe_3O_4 phase in the material. Though in the case of $Mg_{0.2}Ni_{0.8}Fe_2O_4$, the binding energy of Fe $2p_{3/2}$ peak was seen at 710.5 eV, the presence of satellite at 8.0 eV above the main peak ruled out the development of any Fe^{2+} state in the ferrite.

Ni $2p_{3/2}$ peak in Ni ferrite was seen at 855.1 eV. But in case of $Mg_{0.3}Ni_{0.7}Fe_2O_4$ and $Mg_{0.2}Ni_{0.8}Fe_2O_4$ the

peak was seen at 854.3 eV, which is of course higher than that in NiO, but less than that in $NiFe_2O_4$ [20]. The peak shape of Ni $2p_{3/2}$ in $NiFe_2O_4$ and NiO are different, e.g. Ni $2p_{3/2}$ peak in NiO is associated with a shoulder (satellite peak) [20] while that in $NiFe_2O_4$, no such shoulder is reported. So the peak shape of Ni $2p_{3/2}$ (Fig. 5(c)) indicated that Ni was in spinel structure only. The decrease in the peak position in case of Fe $2p_{3/2}$ and Ni $2p_{3/2}$ may be due to cation disorder of Mg^{2+} and Fe^{3+} in tetrahedral and octahedral sites. It may be assumed that Fe^{3+} (B) has (n) Mg^{2+} and $(6-n)$ Fe^{3+} nearest neighbor (A) site cation. In an ideal situation of inverse spinel where $n = 0$ the binding energy of Fe $2p_{3/2}$ peak was at 711.2 eV. But when $n > 0$, some Mg^{2+} enters into the tetrahedral site which changed the binding energy of Fe^{3+} $2p_{3/2}$ photoelectron peak. Similarly, Ni^{2+}, which was surrounded by 6 Fe^{3+} ions in tetrahedral sites, reduced to $6-n$ number of Fe^{3+} and n number of Mg^{2+} cations due to cation disorder. Thus due to cation disorder the distribution of the cations surrounding any site also changes which might be the reason for the reduction in binding energy of Ni $2p_{3/2}$ and Fe $2p_{3/2}$ peaks.

It was observed from the analysis of the Mg–Ni ferrite by XRD and XPS that the composition of the ferrite formed by the solid state reaction, under the condition used in the present study, varied along the depth of the grain. Such non-uniformity towards the depth of the ferrite grains was seen in case of bimetallic ferrite systems [9], it was discussed as surface enrichment process. The surface enrichment process occurred due to different mobility of the cations in the oxygen lattice during the formation and growth of spinel. In the case of $Mg_xNi_{(1-x)}Fe_2O_4$ ferrite, the enrichment phenomenon is very significant. From the data on the temperature of formation of $NiFe_2O_4$ and $MgFe_2O_4$, it is known that $NiFe_2O_4$ is formed at lower temperature (950 °C) than $MgFe_2O_4$ (1200 °C). So, during the process of heating (at the rate 3 °C/min), the solid state reactions of Ni with α-Fe_2O_3 and Mg with α-Fe_2O_3 occur at different rates. Magnesium ions are very sensitive towards heat treatment due to its high mobility, whereas distribution of Ni^{2+} normally does not show much dependence on temperature due to its high preference for octahedral site. Thus, it is evident from the results that during the reaction, the nucleation of the Ni ferrite took place first and then Mg^{2+} segregated at the surface of the Ni ferrite. On attaining the higher temperature the Mg^{2+} reacts with Ni ferrite by diffusing into the Ni ferrite grains. As Ni is incorporated into the octahedral site of the spinel, Mg^{2+} was settled either in the octahedral or tetrahedral sites. The higher mobility of Mg^{2+} than Fe^{3+} or Ni^{2+} during reaction caused the enrichment of Mg on the surface.

3.2.3. Sputtering effect on magnesium nickel ferrites

Ferrites normally undergo damage due to sputtering of the surface by Ar ion beam. Such beam damages were reported in case of $NiFe_2O_4$ [21]. Similar effect was also seen in case of $Mg_{0.5}Ni_{0.5}Fe_2O_4$ (Fig. 5). The sputtering effect was seen prominently in case of Ni $2p_{3/2}$ (Fig. 5(b)) and Fe $2p_{3/2}$ (Fig. 5(a)) peaks. The satellite peak for Fe $2p_{3/2}$ peak in $MgFe_2O_4$ vanished after sputtering which indicated the reduction of the Fe^{3+} to Fe^{2+} or to Fe^0 due to sputtering [22]. The binding energy of the Fe $2p_{3/2}$ peak was also reduced that indicated the presence of both Fe^{2+} and Fe^{3+} states on the surface after sputtering. The binding energy of Ni $2p_{3/2}$ peak was also reduced due to sputtering. In Fig. 5(b), pure Ni^0 appeared as a shoulder at 2.9 eV below the Ni ferrite peak. However such effect was not seen distinctly in case of Mg 1s photoelectron peak. The peak width of the Mg 1s peak was reduced to 1.8 eV from 2.7 eV after sputtering. This may be due to alteration introduced by the ion beam in the lattice surrounding the Mg^{2+} in the ferrite.

4. Conclusions

$MgFe_2O_4$ and $Mg_xNi_{(1-x)}Fe_2O_4$ prepared by solid state method were characterized by XRD. A plot of lattice parameter versus composition of the ferrites ($Mg_xNi_{(1-x)}Fe_2O_4$, $x \leqslant 1$) observed to follow linearity. The deviation of lattice parameter of $MgFe_2O_4$ from the linear plot was explained in terms of the distribution of Mg^{2+} in the octahedral and tetrahedral sites of the spinel lattice which might have resulted in an increase in its lattice parameter.

XPS technique was used extensively to characterize the Mg and Mg–Ni ferrites. Mg enrichment was observed in the $Mg_xNi_{(1-x)}Fe_2O_4$ and the enrichment increased with Mg content (x). In case of pure $MgFe_2O_4$ the peak position was found at 1303.1 eV which is lower than the Mg 1s binding energy in MgO (1303.6 eV). In some Mg–Ni ferrite, the Mg 1s peak was found broader than that in $MgFe_2O_4$. The increase in FWHM was explained in terms of the cation distribution of Mg^{2+} in octahedral and tetrahedral sites of the oxygen lattice. Mg in tetrahedral site was found at 1302.1 eV in photoelectron spectra of quenched $MgFe_2O_4$ or $Mg_xNi_{(1-x)}$-Fe_2O_4, (with composition $x = 0.5$ or less).

In Mg rich Mg–Ni ferrite Ni $2p_{3/2}$ peak was seen at 855.1 eV, but in Ni rich Mg–Ni ferrite the peak position reduced to around 854.3 eV. The change in Ni $2p_{3/2}$ binding energy was explained as due to the cation disorder of Mg^{2+} and Fe^{3+} in the interstitial sites of the oxygen lattice.

Extensive analysis of the cation distribution in the case of $Mg_xNi_{(1-x)}Fe_2O_4$ is able to give an insight into the stability of these systems. Thus the passivation behavior of the film containing Mg–Ni ferrites is correlatable to metal release behavior. This present study in that sense has formulated base criteria for such correlation.

References

[1] J.A. Sawicki, H.A. Allsop, J. Nucl. Mater. 240 (1996) 22.
[2] C.C. Lin, F.R. Smith, Y. Uruma, T. Taneichi, N. Ichikawa, in: Proceedings of JAIF International Conference on Water Chemistry of Nuclear Reactor System, vol. II, 1988, p. 386.
[3] S. Velmurugan, S. Padma, S.V. Narasimhan, P.K. Mathur, P.N. Moorthy, J. Nucl. Sci. Technol. 33 (1996) 641.
[4] D. Hiroishi, K. Ishigure, International Conference on Water Chemistry in Nuclear Plants, JAIF-98, 1998, p. 116.
[5] H.St.C. O'Neill, H. Annersten, D. Virgo, Am. Mineral. 77 (1992) 725.
[6] G. Allen, J.A. Jutson, P.A. Tempest, J. Nucl. Mater. 158 (1988) 96.
[7] A.A.M. Prince, S. Velmurugan, S.V. Narasimhan, C. Ramesh, N. Murugesan, P.S. Raghavan, R. Gopalan, J. Nucl. Mater. 289 (2001) 281.
[8] S. Bera, A.A.M. Prince, S. Velmurugan, P.S. Ranganathan, R. Gopalan, G. Paneerselvam, S.V. Narasimhan, J. Mater. Sci. 36 (2001) 5379.
[9] G.C. Allen, K.R. Hallam, Appl. Surf. Sci. 93 (1996) 25.
[10] D.K. Sarkar, S. Bera, S.V. Narasimhan, S. Dhara, K.G.M. Nair, S.C. Chaudhury, Appl. Surf. Sci. 120 (1997) 159.
[11] V. Sepelak, D. Baabe, F.J. Litterst, K.D. Becker, J. Appl. Phys. 88 (2000) 5884.
[12] E. De Grave, C. Dauwe, A. Govaert, J. De Sitter, Phys. Status Solidi B 73 (1976) 527.
[13] JCPDS card no. 360398.
[14] R.D. Shannon, Acta Crystallogr. A 32 (1976) 751.
[15] A. Roy, J. Ghoshe, A. Roy, R. Ranganathan, Solid State Commun. 103 (1997) 269.
[16] Ravindran, K.C. Patil, J. Mater. Sci. 22 (1987) 3261.
[17] H. Seyama, M. Sama, J. Chem. Soc. Faraday Trans. 180 (1984) 237.
[18] N.S. McIntyre, M.G. Cook, Anal. Chem. 47 (1975) 2208.
[19] K. Seshan, A.L. Sashimohan, D.K. Chakraborty, A.B. Biswas, Phys. Status Solidi 68 (1981) 97.
[20] C.D. Wagner, W.M. Riggs, L.E. Davis, J.F. Moulder, G.E. Muilenberg, Handbook of XPS, PE Corporation, USA, 1979.
[21] M.P. Srinivasan, S. Bera, S.V. Narasimhan, J. Mater. Sci. Technol. 15 (1999) 473.
[22] T.J. Chung, C.R. Brundle, K. Wandelt, Thin Solid Films 53 (1978) 79.